Hamling, I. J., D'Anastasio, E., Wallace, L. M., Ellis, S., Motagh, M., Samsonov, S., Palmer, N., Hreinsdóttir, S. (2014):Crustal deformation and stress transfer during a propagating earthquake sequence: The 2013 Cook Strait sequence, central New Zealand. - *Journal of Geophysical Research*, *119*, 7, p. 6080-6092

DOI: http://doi.org/10.1002/2014JB011084

AGU PUBLICATIONS

JGR

Journal of Geophysical Research: Solid Earth

RESEARCH ARTICLE

10.1002/2014JB011084

Key Points:
- Slip models for Cook Strait and Lake Grassmere earthquakes, New Zealand
- Models suggest that stress transfer played an important role in triggering events

Supporting Information:
- Readme
- Figure S1
- Figure S2
- Table S1
- Table S2
- Table S3
- Data S1
- Data S2

Correspondence to:
I. J. Hamling,
I.Hamling@gns.cri.nz

Citation:
Hamling, I. J., E. D'Anastasio, L. M. Wallace, S. Ellis, M. Motagh, S. Samsonov, N. Palmer, and S. Hreinsdóttir (2014), Crustal deformation and stress transfer during a propagating earthquake sequence: The 2013 Cook Strait sequence, central New Zealand, *J. Geophys. Res. Solid Earth*, *119*, 6080–6092, doi:10.1002/2014JB011084.

Received 3 MAR 2014
Accepted 28 JUN 2014
Accepted article online 1 JUL 2014
Published online 24 JUL 2014

Crustal deformation and stress transfer during a propagating earthquake sequence: The 2013 Cook Strait sequence, central New Zealand

I. J. Hamling[1], E. D'Anastasio[1], L. M. Wallace[2], S. Ellis[1], M. Motagh[3], S. Samsonov[4], N. Palmer[1], and S. Hreinsdóttir[1]

[1]GNS Science, Lower Hutt, New Zealand, [2]Institute for Geophysics, University of Texas at Austin, Austin, Texas, USA, [3]GFZ German Research Centre for Geosciences, Potsdam, Germany, [4]Natural Resources Canada, Ottawa, Ontario, Canada

Abstract The 2013 Cook Strait earthquake sequence began on 18 July 2013 with two foreshocks of M_w 5.7 and M_w 5.8 and culminated in the M_w 6.6 Cook Strait and Lake Grassmere events on 21 July and 16 August, respectively. Located ~50 km south of New Zealand's capital, Wellington, the earthquakes generated the most significant ground shaking in the Wellington and Marlborough regions in recent decades. During the first event, located under Cook Strait, continuously recording GPS instruments across central New Zealand recorded up to 5 cm of horizontal displacement. Modeling suggests that the rupture was 25 km long with up to 90 cm of dextral strike slip. The second event, located 20 km to the southwest, caused displacements of up to 25 cm at GPS sites located around the Clifford bay area. In addition, two interferograms from RADARSAT-2 and TerraSAR-X showed up to 30 cm of line-of-sight displacement in the vicinity of Lake Grassmere. Modeling indicates predominantly dextral strike slip of up to 2.1 m. Coulomb Stress changes induced by the earlier foreshocks suggest that the Cook Strait event was triggered by the preceding events and that the Lake Grassmere event was subsequently triggered by the Cook Strait earthquake.

1. Introduction

The 2013 Cook Strait earthquake sequence began on 18 July with two earthquakes, located beneath the Cook Strait (Figure 1), with magnitudes of M_w 5.7 and 5.8. Focal mechanisms, from regional moment tensor inversions [*Ristau*, 2013], suggest thrust mechanisms for these events with hypocentral depths of ~20 km. Three days later, on 21 July, a M_w 6.6 (the Cook Strait earthquake) occurred ~50 km south of New Zealand's capital, Wellington. The moment tensor solutions suggested an almost pure right lateral rupture at a depth of 16 km. It was followed by at least ~2500 aftershocks, >M_w 2, (Figure 1) extending over a ~25 km NE-SW trending region. On 16 August a second M_w 6.6 (the Lake Grassmere earthquake), located beneath the Clifford bay region at the north eastern tip of the South Island, ~10 km east of Seddon (Figure 1), occurred causing widespread shaking across the Marlborough and Wellington regions. As with the previous event, the moment tensor solution suggested predominantly right lateral slip with a hypocentral depth of ~8 km.

Here we present GPS and Satellite Radar Interferometry (InSAR) coseismic observations for the Cook Strait and Lake Grassmere events. Using elastic dislocation models, we estimate the slip during the two events and investigate the interaction between the Cook Strait and Lake Grassmere sequence. The sequence has important implications on the interaction between slab events along the Hikurangi margin and events in the overriding plate as well as provide insights into the tectonics of a region transitioning between subduction in the north to strike-slip faulting to the south.

2. Tectonic Setting of Central New Zealand

The tectonics of New Zealand is largely controlled by the convergence of the Australian and Pacific plates at rates of 39–48 mm/yr [*Beavan et al.*, 2002]. Along-strike variations of the plate boundary and relative motion between the plates has lead to a change from predominantly subduction of the Pacific plate beneath the North Island to strike-slip faulting in the Marlborough in the northern South Island. In the North Island, partitioning of the margin normal and margin parallel relative plate motions is accommodated along the subduction thrust [*Nicol and Beavan*, 2003; *Wallace et al.*, 2004] and by a combination of strike slip-faulting

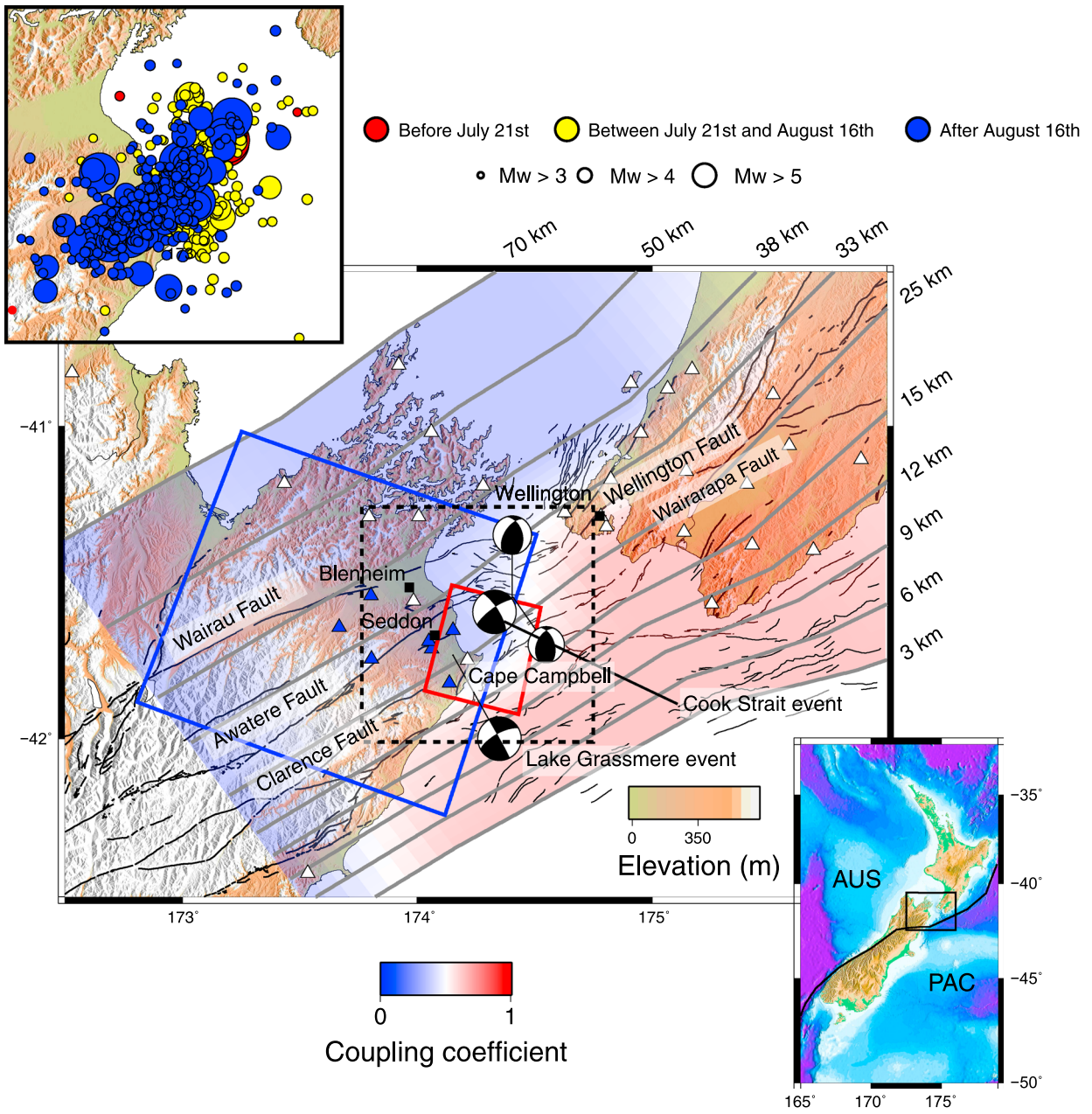

Figure 1. Color-shaded relief map of central New Zealand. The inset shows the location of the plate boundary between the Pacific (PAC) and Australian (AUS) plates. In the main figure, the blue and red boxes show the outline of the RADARSAT-2 and TerraSAR-X radar frames used in this study, respectively. The white triangles are the location of the continuous GPS sites used in the joint inversion, and the blue triangles are the location of the campaign sites. The dashed black box is the region shown in the inset in the top left of the figure highlighting the earthquakes during the sequence. Red, yellow, and blue circles show the location of earthquakes from 1 June before the Cook Strait event, between the Cook Strait and Lake Grassmere events, and after the Lake Grassmere event, respectively. Moment tensor solutions are shown for the two foreshocks and the Cook Strait and Lake Grassmere events. Overlain is the slip rate deficit on the subduction interface *Wallace et al.* [2012], the red regions indicate the locked zone. The gray lines indicate the depth to the interface.

and rotation of the fore arc [*Walcott*, 1984; *Beanland and Haines*, 1998; *Wallace et al.*, 2004], respectively. In the vicinity of the Cook Strait, the right lateral Wairarapa (8–12 mm/yr), Wellington (6–7 mm/yr), and Ohariu (1–2 mm/yr) faults accommodate ~20 mm/yr of margin parallel motion [*Beanland and Haines*, 1998; *Van Dissen and Berryman*, 1996; *Little et al.*, 2009; *Carne et al.*, 2011].

Across the Cook Strait into the north of the South Island, most of the plate motion is taken up along four major strike-slip faults which form part of the Marlborough Fault system [*Holt and Haines*, 1995; *Van Dissen and Yeats*, 1991] (Figure 1). Slip rates in the range of 4 to 8 mm/yr are observed along the Awatere, Clarence,

and Wairau faults [*Benson et al.*, 2001; *Mason et al.*, 2006; *Zachariasen et al.*, 2006; *Van Dissen and Nicol*, 2009]. The southern most fault, the Hope fault, is New Zealand's second fastest slipping onshore fault at rates of 13–23 mm/yr [*Van Dissen and Yeats*, 1991; *Langridge and Berryman*, 2005]. South of the Marlborough fault zone, slip is transferred onto the Alpine Fault [*Van Dissen and Yeats*, 1991; *Holt and Haines*, 1995], which accommodates 70–75% of the Pacific-Australia relative motion [e.g., *Norris and Cooper*, 2001; *Sutherland et al.*, 2006].

The transition from faulting along the North Island dextral fault belt to the Marlborough fault system is poorly understood. The Cook Strait, separating the North and South Islands of New Zealand, lies at the junction of the Marlborough fault system, the North Island dextral fault belt, and the Hikurangi subduction zone [*Pondard and Barnes*, 2010]. Faults within the Cook Strait, including the Boo Boo, Cloudy, and Vernon faults, accommodate most of the plate motion. Shallow seismicity, associated with the offshore continuation of inland crustal faults, is quite abundant with prominent clustering along vertical extensions in the Cape Campbell region [*Du et al.*, 2004]. Many of the major faults in the North and South Island were thought to connect through the Cook Strait [e.g., *Lensen*, 1958; *Stevens*, 1974]. Although seismic data have shown that some of these faults, including the Wairau, Awatere, and Wellington faults, do extend offshore into the Cook Strait [*Nodder et al.*, 2007; *Barnes et al.*, 1998; *Mountjoy et al.*, 2009], it is not thought that they form through going structures [*Pondard and Barnes*, 2010]. However, it is likely that they are kinematically linked [*Wallace et al.*, 2012].

3. Data and Modeling

3.1. GPS Data

Coseismic displacements for the Cook Strait and Lake Grassmere earthquakes were recorded by continuously operating GPS stations (cGPS) and campaign GPS stations (sGPS) (Figure 1). Continuous GPS stations (GeoNet, http://geonet.org.nz, and PositioNZ, http://apps.linz.govt.nz/positionz) were available for both the Cook Strait and Lake Grassmere events. Following the Cook Strait event, seven campaign sites were installed and subsequently recorded coseismic offsets for the Lake Grassmere event. An additional five campaign sites, which were not remeasured following the Cook Strait event recorded the combined displacement for both events.

Continuous and campaign GPS data have been processed with Bernese 5.0 software. The processing strategy is an updated version of that described in *Wallace et al.* [2012, and references therein]. Data have been processed holding IGS2008 final orbits and Earth orientation parameters fixed. Absolute receiver and satellite antenna phase patterns are used. Ocean loading coefficients are estimated after Topex model 7.1 (www.oso.chalmers.se). Tropospheric delay is estimated using the Niell mapping functions. Ambiguities are fixed with a quasi-ionosphere-free strategy, using global ionosphere models produced by the Centre for Orbit Determination in Europe (CODE, www.aiub.unibe.ch). Daily solutions are then aligned to ITRF2008 using a three-parameter Helmert transformation onto a subset of IGS stations in the Australian and Pacific area. Uncertainties are estimated by multiplying the chi-square per degree of freedom and RMS error values, resulting from the alignment of the loosely constrained solution to ITRF2008, by a scale factor of 4.

Coseismic offsets for the 21 July Cook Strait event (Figure 2 and Table S1 in the supporting information) are obtained using 10 days of data prior to the earthquake, in order to get a good a priori position, and data from 05:30 to 23:59 of 21 July, discarding the preearthquake observations to avoid biases in the resulting coseismic displacement. Due to the lack of any discernible vertical offsets, we only use the horizontal component of the GPS displacement field. Coseismic GPS displacements due to the 16 August Lake Grassmere event (Figures 3g and 3h, and Tables S2 and S3) have been obtained with a slightly different strategy, to make them comparable to InSAR image acquisition dates. For the August earthquake, we estimate the cumulative offset for both the horizontal and vertical components between 27 July 2013 and 20 August 2013. To isolate the coseismic offsets, we use the long-term cGPS time series to estimate the annual and semiannual periodicities, interseismic motion, and early postseismic decay [*Langbein*, 2008] due to Cook Strait and Grassmere events. For sGPS sites we use the velocity model of *Wallace et al.* [2012], derived from ~800 campaign 65 continuous GPS stations measured since the early 1990s, to account for interseismic motion since the last measured epoch. For the seven sGPS sites used in the inversion, which were measured between 26 July 2013 and 7 August 2013 prior to the Lake Grassmere earthquake and remeasured between 23 August 2013 and 12 September 2013, the interseismic motion is negligible.

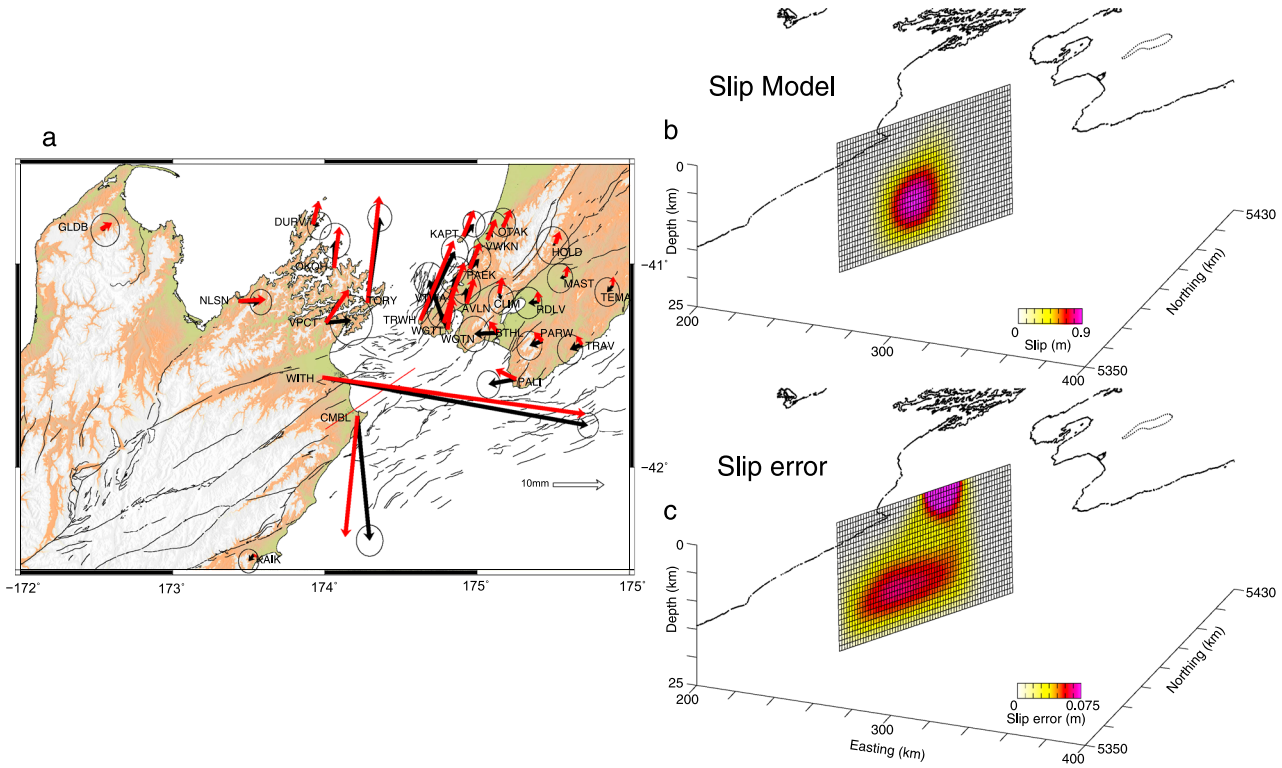

Figure 2. (a) Observed (black) and modeled (red) horizontal displacements from the Cook Strait earthquake. Blue line shows the surface trace of the mode. (b) Best fit distributed slip model for the Cook Strait earthquake generated from the inversion of horizontal GPS displacements. (c) One σ slip error projected onto the modeled fault plane.

3.2. InSAR Data

Satellite Radar Interferometry (InSAR) is a widely used technique for monitoring deformation of the Earth's surface [e.g., *Massonnet et al.*, 1993; *Jónsson et al.*, 2002; *Elliott et al.*, 2012]. By differencing the phase from two radar images acquired at different times, maps of range change between the radar and ground can be obtained [e.g., *Massonnet and Feigl*, 1998]. Following the Cook Strait earthquake, RADARSAT-2 and TerraSAR-X data (Table 1) were acquired over the Cape Campbell area (Figure 1) and used to form two coseismic interferograms covering the 16 August Lake Grassmere event. For RADARSAT-2, images were acquired on 27 July and 20 August on a descending pass with an incidence angle of ~44° and perpendicular baseline of 27 m. TerraSAR-X images were also acquired in a descending pass on 3 and 25 August, with an incidence angle of ~24° and perpendicular baseline of 22 m. Processing of the RADARSAT-2 data was done using GAMMA [*Wegmüller and Werner*, 1997], topographic corrections were made using a 30 m ASTER DEM, and the interferogram was filtered using a power spectrum filter [*Goldstein and Werner*, 1998]. For TerraSAR-X, data were processed using SARScape with topographic corrections made using a 3 arc sec (90 m) digital elevation model (DEM) generated by the NASA Shuttle Radar Topography Mission [*Farr and Kobrick*, 2000]. Both interferograms were unwrapped using the Minimum Cost Flow algorithm [*Costantini*, 1998].

3.3. Method to Invert for GPS and InSAR for Coseismic Slip

Each of the earthquakes was modeled individually as a set of rectangular dislocation in an elastic half space [*Okada*, 1985]. For the Cook Strait event, the geometry of the fault plane was initially constrained by performing a hybrid Monte Carlo downhill simplex inversion, which minimizes the square misfit between the observed and calculated displacements at each GPS site [*Wright et al.*, 1999]. We solve for the position, dip, rake, and strike of the dislocation, while fixing its length and depth extent to match the moment tensor solution (Table 2). Parameter uncertainties are calculated using a Monte Carlo simulation in which the 1 σ GPS errors are used to perturb the observations 1000 times (Figure S1 in the supporting information). Comparing the best fit position of the Cook Strait event with the phase discontinuity in the InSAR data suggests that the ruptures were likely to have occurred on the same structure given the similarity in their location

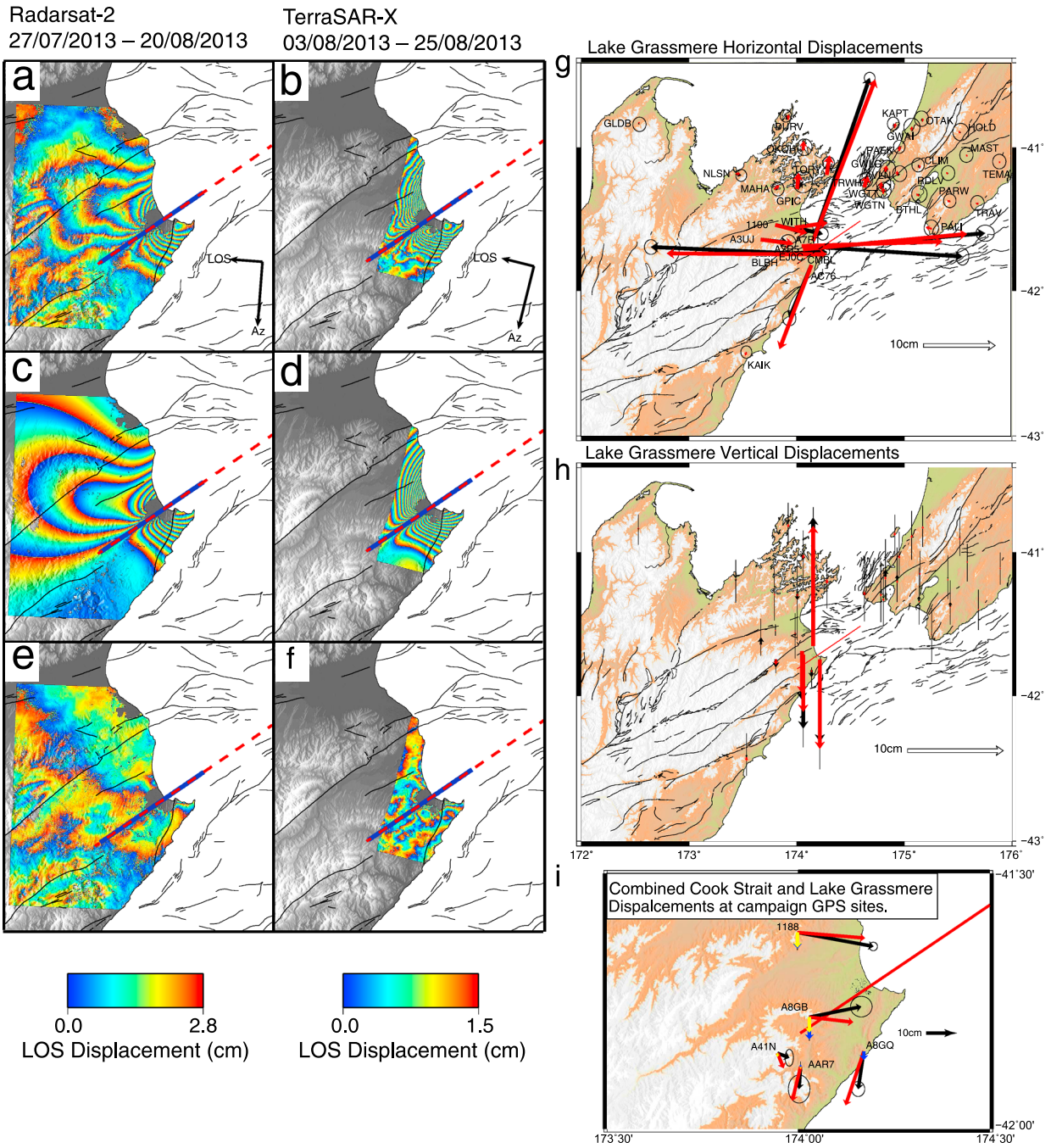

Figure 3. (a,b) RADARSAT-2 and TerraSAR-X interferograms for the Lake Grassmere earthquake. Arrows indicate the flight (Az) and look (LOS) directions. Blue and red dashed lines show the surface trace of the faults for the Lake Grassmere and Cook Strait events, respectively. (c,d) Simulated interferograms for RADARSAR-2 and TerraSAR-X derived from the distributed slip model shown in Figure 4. (e,f) Residual interferograms, generated by subtracting the simulated interferograms from the data. (g) Observed (black) and modeled (red) horizontal GPS displacements from the Lake Grassmere earthquake. Blue line shows the surface trace of the best fit fault. (h) Observed (black) and modeled (red) vertical GPS displacements from the Lake Grassmere earthquake. (i) Observed and modeled cumulative displacements for the Cook Strait and Lake Grassmere earthquakes at five sGPS sites. Black and dark gray arrows show the observed horizontal and vertical displacements, respectively. Red and yellow arrows show the predicted displacement for the horizontal and vertical components.

and strike (Figure S1). Therefore, the strike (234°± 0.7), dip (74.9°± 1.5) and position of the faults, which are consistent with the moment tensor solutions and distribution of aftershocks, are assumed to be the same for both events (Table 1). For each event, we discretize the fault plane into 1 × 1 km patches and allow slip to occur down to 25 km, the depth to the subduction interface in the region. For the Cook Strait event, we fix the rake of each patch to 180°, as suggested by the uniform slip model. In order to fit the InSAR data for

Table 1. Acquisition and Processing Parameters for the InSAR Datasets

Satellite	Beam	Incidence Angle	Resolution	Perp. Baseline	Temp. Baseline	Filter Strength
RADARSAT-2	S6	44.2	~50 m	27	24	0.8
TerraSAR-X	Stripmap	24	~25 m	22	22	0.8

the Lake Grassmere event, we solve for variable rake on each of the patches. Before inverting the data, the interferograms are first subsampled using a Quadtree algorithm [e.g., *Jónsson et al.*, 2002], which reduces the number of data points from $\sim 10^7$ to $\sim 10^3$. To account for the different quantities and uncertainties, the inversion is weighted using the data variance-covariance matrix (VCM). For the InSAR data, the VCM was derived by fitting a 1D covariance function to phase data away from the earthquake [e.g., *Parsons et al.*, 2006]. For the RADARSAT-2 and TerraSAR-X data we find a maximum σ of 9.4 mm and 5.9 mm with *e*-folding lengths of 5 and 1.8 km, respectively. For the GPS data, we weight each data point by the inverse of its variance and assume that there is no correlation between each site. In addition, we vary the relative weighting of each data set and assess the effect on the RMS misfit [*Pedersen et al.*, 2003]. Increasing the weight of the GPS data relative to the InSAR shows little improvement to the fit for the GPS data but causes a significant increase in the misfit with the InSAR data. A good compromise can be made by giving equal weights to both data sets whereby a good fit to both GPS and InSAR data is achieved based on the VCM. Using a Poisson's ratio of 0.25 and a depth-averaged shear modulus (weighted by layer thickness) of 30 GPa, derived from a 3D velocity model [*Eberhart-Phillips et al.*, 2010], we solve for the best fitting slip distribution, **m**, using a nonnegative least-squares inversion [*Bro and Jong*, 1997] by solving the following equation:

$$\begin{pmatrix} \mathbf{A_{tsx}} & \mathbf{x} & \mathbf{y} & 1 & 0 & 0 & 0 & 0 & 0 & 0 \\ \mathbf{A_{rds}} & 0 & 0 & 0 & \mathbf{x} & \mathbf{y} & 1 & 0 & 0 & 0 \\ \mathbf{A_{gpsx}} & 0 & 0 & 0 & 0 & 0 & 0 & 1 & 0 & 0 \\ \mathbf{A_{gpsy}} & 0 & 0 & 0 & 0 & 0 & 0 & 0 & 1 & 0 \\ \mathbf{A_{gpsz}} & 0 & 0 & 0 & 0 & 0 & 0 & 0 & 0 & 1 \\ \boldsymbol{\kappa\nabla^2} & 0 & 0 & 0 & 0 & 0 & 0 & 0 & 0 & 0 \end{pmatrix} \begin{pmatrix} \mathbf{m} \\ a_{\mathrm{tsx}} \\ b_{\mathrm{tsx}} \\ c_{\mathrm{tsx}} \\ a_{\mathrm{rds}} \\ b_{\mathrm{rds}} \\ c_{\mathrm{rds}} \\ c_{\mathrm{gpsx}} \\ c_{\mathrm{gpsy}} \\ c_{\mathrm{gpsz}} \end{pmatrix} = \begin{pmatrix} \mathbf{d_{tsx}} \\ \mathbf{d_{rds}} \\ \mathbf{d_{gpsx}} \\ \mathbf{d_{gpsy}} \\ \mathbf{d_{gpsz}} \\ 0 \end{pmatrix}, \quad (1)$$

where $\mathbf{A}_{\mathrm{tsx}}$, $\mathbf{A}_{\mathrm{rds}}$, $\mathbf{A}_{\mathrm{gpsx}}$, $\mathbf{A}_{\mathrm{gpsy}}$ and $\mathbf{A}_{\mathrm{gpsz}}$ are a set of matrices representing Green's functions for the TerraSAR-X and RADARSAT-2 interferograms, GPS displacements in the *x*, *y*, and *z* directions which, multiplied by **m** produce the model displacements at the observation points, **x** and **y**, using the elastic dislocation formulation of *Okada* [1985]. ∇^2 is the finite difference approximation of the Laplacian operator, which acts to smooth the distribution of slip, the relative importance of which is governed by the size of the scalar smoothing factor κ (Figure S2); *a* and *b* are phase ramps in the *x* and *y* direction respectively to account for residual orbital errors; *c* are offsets to account for the unknown zero phase level (InSAR) or displacements at the reference GPS station (subscripts indicate data source); and **d** is a vector containing the observed displacements. For the Cook Strait event, where only the horizontal GPS displacements are used, the equation reduces by removing the irrelevant rows.

3.4. Cook Strait and Lake Grassmere Slip Models

During the Cook Strait event, maximum horizontal displacements were observed at the northern end of the South Island with up to ~5 cm of eastward motion at WITH (Figure 2). A GPS station located on Cape

Table 2. Comparison Between Different Moment Tensor and Geodetic Fault Parameters

Fault source	Strike	Dip	Rake	Moment
Cook Strait regional MT	234	76	164	6.6
GCMT Cook Strait	234	76	164	6.5
Cook Strait geodetic solution	234	74	179	6.6
Lake Grassmere regional MT	241	70	179	6.6
GCMT Lake Grassmere	238	69	167	6.5
Lake Grassmere geodetic solution	234	74	168	6.7

Table 3. RMS Misfit for Each Data Set[a]

Earthquake	RMS_{rds}	RMS_{tsx}	RMS_{gpsx}	RMS_{gpsy}	RMS_{gpsz}
Cook Strait	-	-	2.5	1.8	-
Lake Grassmere	17	13	8	9	5

[a]Subscript indicates data source.

Campbell (CMBL) observed ~2.5 cm of southward motion, consistent with a right lateral strike-slip earthquake, and displacements of ~1 cm were observed on the lower North Island, close to Wellington. The best fit model (Figure 2), from the inversion of horizontal GPS displacements, suggests that the earthquake rupture was ~25 km long, with a slip of more than 30 cm extending from 7 to 24 km deep. Maximum slip of 90 cm is estimated at ~14–16 km depth, in accordance with the hypocentral depth from moment tensor solutions, giving a geodetic moment equivalent to a M_w 6.6 earthquake. The model explains most of the observed deformation, RMS to the east and north components of 2.5 and 1.8 mm, respectively (Table 3). To assess the distribution of model parameters, we perform a bootstrap resampling procedure [*Segall*, 2002] to generate 1000 new data sets and reinvert for the distribution of slip (Figure 2). The 1 σ errors, in the region of maximum slip, are less than 5 cm. At the northern end of the modeled fault, where the distribution of data points is more sparse, the 1 σ is ~10 cm.

Deformation associated with the August 2013 Lake Grassmere earthquake was largely concentrated on the South Island with small (~1 cm) displacements observed at GPS on the North Island. Campaign GPS sites located in the vicinity of Lake Grassmere show up to 26 cm of eastward and 15 cm of vertical displacement (Figures 3g and 3h). The continuous GPS site CMBL, located on Cape Campbell, was displaced westward by ~24 cm and subsided by 8 cm. InSAR observations show ~30 cm of LOS range change on Cape Campbell and to the north of Lake Grassmere (Figure 3).

The joint inversion of InSAR and GPS suggests slip of up to 2.1 m at 7–9 km depth (Figure 4). The best fit model suggests that the region of slip was ~18 km long and extending from 3 to 15 km depth, straddling the coast line (Figure 4). The model predicts predominantly right lateral slip, with a small thrust component (mean rake 168°), and a geodetic moment equivalent to a M_w 6.7 earthquake. The larger predicted magnitude is likely to be a result of the longer time period covered by the InSAR data, some aftershocks and afterslip following the earthquake will be modeled as slip leading to a larger slip estimate. The model explains 98% of the total data variance and gives a RMS misfit of 17, 13, 8, 9, and 5 mm to the RADARSAT-2, TerraSAR-X, GPS east, north, and vertical components, respectively (Table 3). Larger residuals of up to 3.5 cm are observed in the horizontal displacements at campaign GPS sites close to the fault, and residual fringes are observed around Lake Grassmere and the coast (Figure 3). Areas around the lake suffered from liquefaction and numerous landslides [*Van Dissen et al.*, 2013] and, given that the area is made up of lagoonal deposits and sands, it is likely that some of the observed residuals are due to the local geology. As with the Cook Strait event, we perform a bootstrap analysis of 1000 new data sets to estimate the errors in the slip distribution. The 1 σ errors for the dip-slip and strike-slip components are less than 12 and 15 cm respectively (Figure 4).

Using the slip models for both the Cook Strait and Lake Grassmere events, we also compute the summed displacement at the five sGPS sites, which were not used in the inversion, but contained both the Cook Strait and Lake Grassmere events (Figure 3i). The modeled displacements from both events provide a good fit to the observed displacements at the sGPS sites with an RMS misfit of 12, 21, and 12 mm to the east, north, and vertical components. Some of the difference is likely to arise from the removal of the interseismic model as these sites were previously measured in early 2012.

4. Stress Transfer Between the Cook Strait Events

To investigate the potential triggering relationships between the different events during the Cook Strait and Lake Grassmere sequence we use the distributed slip models presented earlier to calculate the Coulomb failure stress (ΔCFS) along each of the modeled fault plane. For the Cook Strait event, we use two simple rectangular sources to represent the M_w 5.7 and 5.8 earthquakes, consistent with the parameters from the moment tensor solutions, to induce a stress change along the modeled fault plane. Similarly, we use the slip distribution for the Cook Strait event and resolve the stress onto the fault plane of the Lake Grassmere event

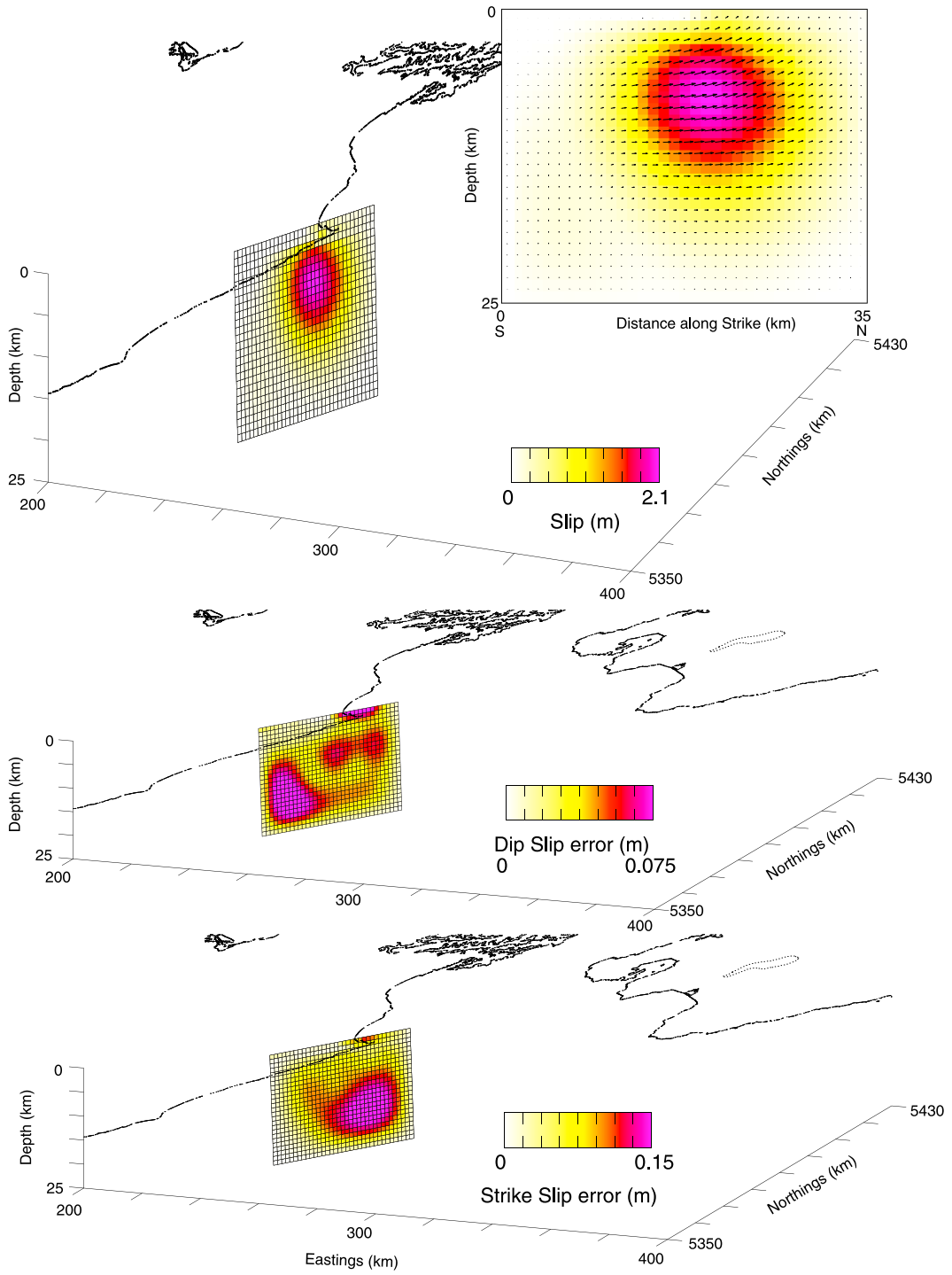

Figure 4. (top) Best fit distributed slip model for the Lake Grassmere earthquake. Subfigure shows the slip distribution along the plane with arrows showing the direction of slip on each patch. (middle) One σ error for the dip-slip component along the modeled fault plane. (bottom) One σ error for the strike-slip component along the modeled fault plane.

assuming the average rake of 168°. We follow the method of [*Hamling et al.*, 2010] to calculate and rotate the internal stress field, onto the relevant fault plane. Since the pore pressure for the fault zone is unknown, we use the apparent coefficient of friction, μ', which includes the effects of pore fluids and material properties in the fault zone. Various studies have found that μ' lies between 0 and 0.6 [*Deng and Sykes*, 1997]. Varying the value shows little effect on our results, and for this study we use a value of 0.4.

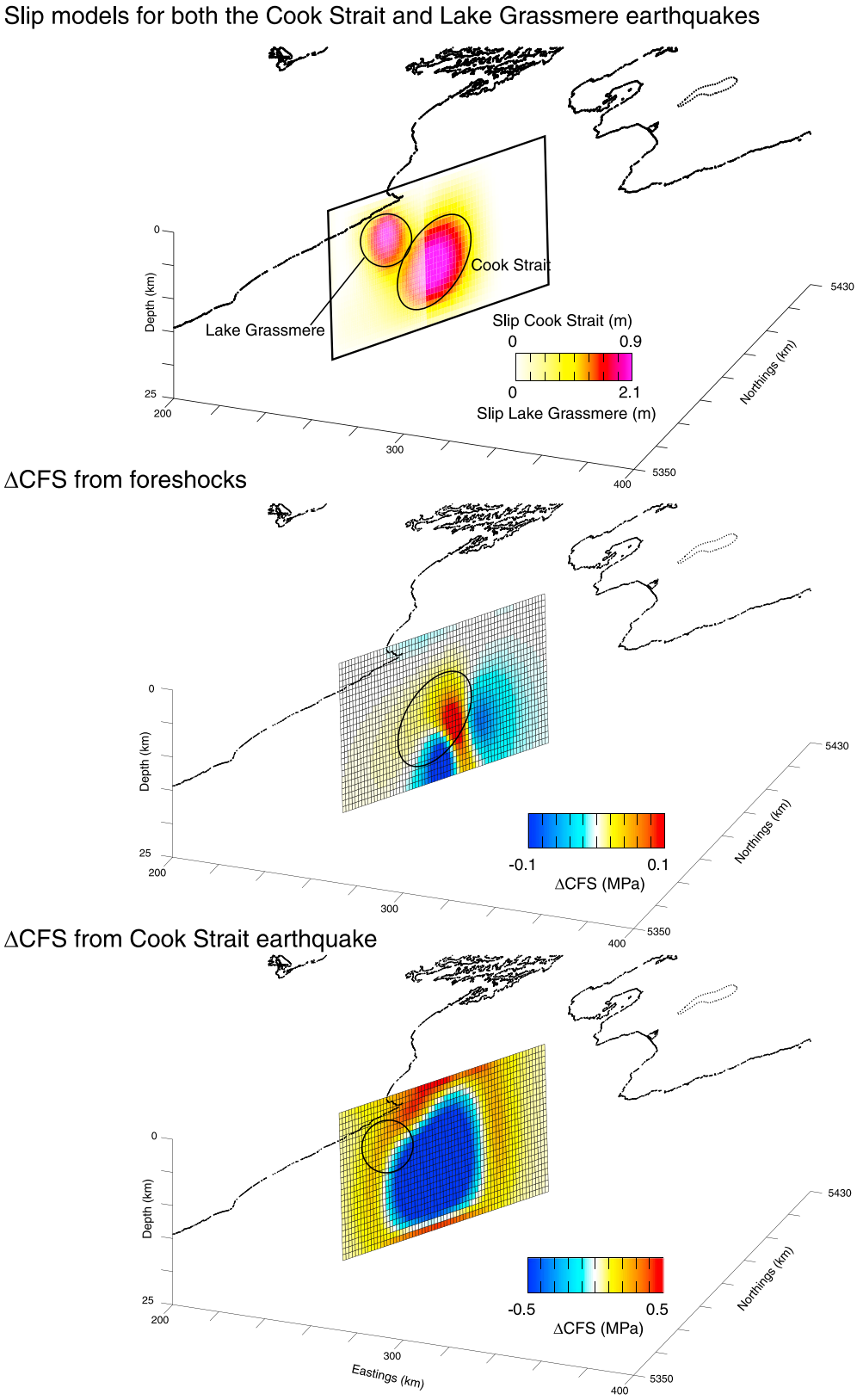

Figure 5. (top) Slip models for the Cook Strait and Lake Grassmere earthquakes. Circles indicate the region of largest slip for each event. (middle) ΔCFS projected onto the Cook Strait fault plane induced by the M_w 5.7 and 5.8 foreshocks. The black circle shows the region of largest modeled slip from the Cook Strait earthquake. (bottom) ΔCFS projected onto the Lake Grassmere fault plane induced by the M_w 6.6 Cook Strait event. The circle shows the region of largest modeled slip.

Based on the moment tensor solutions for the M_w5.7 and 5.8, and a rake of 180° for the Cook Strait event, we find that areas estimated to have slipped by more than 30 cm are generally located within regions where the modeled stress change is greater than 0.01 MPa (Figure 5) and that the area of maximum slip is located where the stresses are increased by ~0.05 MPa. Similarly for the Lake Grassmere event, we find that the majority of estimated slip occurs in regions where the Coulomb failure stress ΔCFS has increased and that, in the regions where maximum slip occurred, the stresses were increased by ~0.25 MPa.

5. Discussion and Conclusions

Analysis and modeling of geodetic data following the Cook Strait and Lake Grassmere events suggest that both events occurred along the same, unmapped, fault which extends from beneath Lake Grassmere into the Cook Strait. Our best fitting fault plane and the distribution of aftershocks (Figure 1) follow a similar strike to the Clarence fault. However, north of its mapped termination, ~20 km southwest of Lake Grassmere, the Clarence fault has no visible surface trace. Therefore, if the Cook Strait and Lake Grassmere events did occur along an unmapped section of the Clarence fault then they must have ruptured a juvenile section of the fault which has not yet broken the overlying strata to produce a surface expression. Previous studies suggest that the termination of dextral slip along the Clarence fault has lead to the strike-slip motion, in the Lake Grassmere region, being accommodated near the surface by the clockwise, vertical axis rotation of a rigid block, bounded by the London Hills fault [*Townsend and Little*, 1998; *Wallace et al.*, 2012]. However, given that both the Cook Strait and Lake Grassmere events were predominantly dextral strike slip, at least some of the dextral shear must be accommodated by strike-slip faulting.

It is now well established that stress transfer from a major earthquake may trigger subsequent earthquakes in nearby regions with stress changes as low as 0.01 MPa triggering seismicity [*Reasenberg and Simpson*, 1992; *King et al.*, 1994; *Harris and Simpson*, 1996]. The stress transfer from the M_w 5.7 and 5.8 foreshocks onto the modeled Cook Strait fault plane suggests that the ΔCFS in the hypocentral region was increased by ~0.05 MPa. The average ΔCFS, as a result of the Cook Strait event in the hypocentral region of the Lake Grassmere event, is ~0.3 MPa and ~70% of the area estimated to have slipped is located in regions where the ΔCFS is calculated to have increased by more than 0.01 MPa. The high correlation between the location of estimated slip and increased ΔCFS suggest that both the Cook Strait and Lake Grassmere events were triggered by the preceding earthquakes. Another consideration for the triggering of the Cook Strait earthquake sequence was an ongoing slow slip event (SSE) along a deep portion of the Hikurangi margin beneath the Kapiti coast [*Wallace et al.*, 2013]. The SSE started at the beginning of 2103 and, at the time of the earthquakes, had an accumulated magnitude equivalent of a ~6.7 M_w earthquake. The largest slip was located at ~30 km depth, ~100 km north of the Cook Strait epicenter. Using the slip distribution for the SSE from *Wallace et al.* [2013] and resolving the stresses onto the foreshock and Cook Strait fault planes, we find that there was an increase in the ΔCFS across all of the modeled fault planes. However, the values are an order of magnitude lower than the suggested triggering threshold of 0.01 MPa [*Harris and Simpson*, 1996]. Although this does not preclude the SSE as a trigger, it seems unlikely that the static stress induced by the SSE is wholly responsible for the Cook Strait sequence.

Despite their similarities, modeling suggests that the Cook Strait event ruptured a larger area but with lower slip compared with the Lake Grassmere event. Assuming a circular rupture for both events, defined by the area slipping by more than 10% of their maximum, would give apparent stress drops ($\frac{7M_0}{16a^3}$, [*Eshelby*, 1957; *Aki*, 1972]) of 1 and 3.5 MPa, respectively. The difference in the apparent stress drop may be an artifact of the inversion given the difference in the smoothing values used for the inversion and the distribution and type of data available for the two events. Only 27 sites recorded noticeable displacements for the Cook Strait event, and only a few on the North and South Islands showed displacements more than 1 cm. For the Lake Grassmere event, there were additional campaign GPS near the rupture and InSAR data which greatly increases the number of data points in the Lake Grassmere region. However, peak horizontal ground accelerations observed near Cape Campbell recorded values of 0.26 g and 0.67 g for the Cook Strait and Lake Grassmere events, respectively [*Holden et al.*, 2013]. Given the similarity between the events, if we assume that the local site effects were the same for both events, then the only difference in the observed acceleration should be a result of the difference in distance from the observation point to the hypocenter. For the Cook Strait and Lake Grassmere events, this distance was ~34 and 16 km respectively. Based on ground motion prediction data from New Zealand [*Stirling et al.*, 2012], the predicted ratio between the peak accelerations for two M_w ~6.6 strike-slip events, located 16 and 34 km apart, would be 1.8. The observed

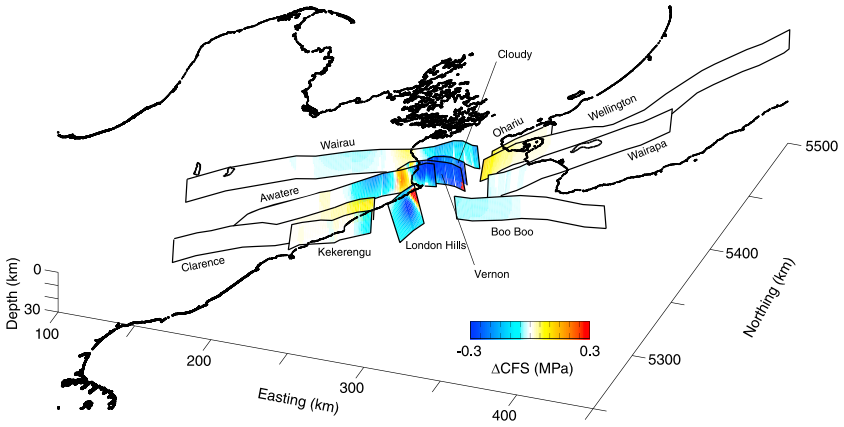

Figure 6. ΔCFS as a result of the Cook Strait and Lake Grassmere events resolved onto the major faults around Cook Strait.

ratio is ~2.5, supporting a larger stress drop during the Lake Grassmere event as suggested by our best fit models.

In addition to the suggested triggering between the two main earthquakes, we use both the Cook Strait and Lake Grassmere slip models to resolve the Coulomb Failure Stress onto mapped faults [*Litchfield et al.*, 2014; *Pondard and Barnes*, 2010] around central New Zealand and onto the Hikurangi subduction interface [*Williams et al.*, 2013]. For all of the crustal faults in Figure 6, the rake is assumed to be for pure right lateral strike slip with the exception of the London Hills fault which has a rake consistent for a thrust fault [*Townsend and Little*, 1998]. For the subduction interface (Figure 7), we set the rake direction equal to a pure thrust. Within the Cook Strait, the majority of the faults show negative stress changes suggesting that they have been taken farther away from failure. This is most notable on the offshore extension of the Vernon fault, where ΔCFS is in the region of −0.5 MPa, and along the Cloudy fault (Figure 6). The southern offshore extension of both the Ohariu and Wellington faults show increased stress changes of ~0.1 MPa, while the Wairapa and Boo Boo faults both show small negative changes. In the South Island, the northern section of the Clarence fault and small sections of the Awatere and Wairau show increases in ΔCFS of ~0.1 MPa. Typically, for a set of parallel or subparallel faults the rupture of one would reduce the stress on neighboring faults [*Robinson*, 2004] as is the general case here. However, in the case of faults located along strike of a rupture, such as the Clarence fault, the expected ΔCFS would be increased.

The ΔCFS resolved onto the subduction interface shows two main regions of increased and decreased stresses. To the east and updip of the Cook Strait and Lake Grassmere events, the stresses on the subduction interface are generally negative (Figure 7). However, areas located directly updip and downdip of the events show increases in ΔCFS, approaching 0.3 MPa, close to the Lake Grassmere event. Downdip, the region of increased stress is broad extending down to ~50–60 km. Updip positive stress changes extend up to the top of the interface. Although the predicted ΔCFS increases are located on parts of the interface where the slip deficit is thought to be low, the coupling along the plate interface is relatively unknown [*Wallace et al.*,

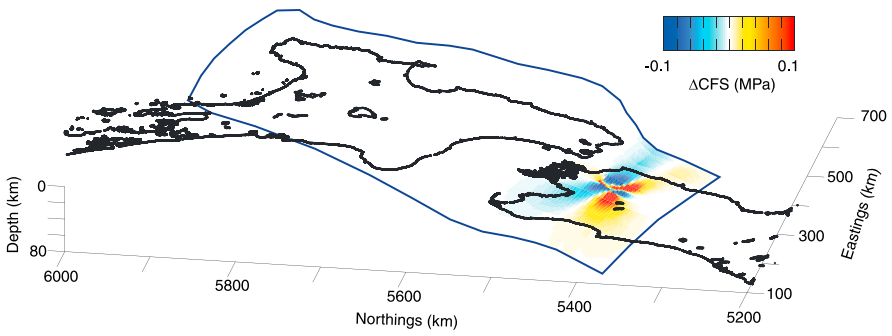

Figure 7. ΔCFS as a result of the Cook Strait and Lake Grassmere events resolved onto subduction interface.

2012]. Therefore, it is likely that the Cook Strait and Lake Grassmere events have loaded a portion of the interface which is thought to have the potential to rupture in an ~M_w 8.5 event [*Wallace et al.*, 2009].

Acknowledgments
The authors would like to thank the Canadian Space Agency and DLR for access to RADARSAT-2 and TerraSAR-X data and Geonet (http://geonet.org.nz) and GEOSYSTEMS NEW ZEALAND Ltd for the GPS data. The ASTER GDEM is the property of METI and NASA.

References

Aki, K. (1972), Earthquake mechanism, *Tectonophysics*, *13*(1), 423–446.
Barnes, P. M., B. M. Lépinay, J.-Y. Collot, J. Delteil, and J.-C. Audru (1998), Strain partitioning in the transition area between oblique subduction and continental collision, Hikurangi margin, New Zealand, *Tectonics*, *17*(4), 534–557.
Beanland, S., and J. Haines (1998), The kinematics of active deformation in the North Island, New Zealand, determined from geological strain rates, *N. Z. J. Geol. Geophys.*, *41*(4), 311–323.
Beavan, J., P. Tregoning, M. Bevis, T. Kato, and C. Meertens (2002), Motion and rigidity of the Pacific Plate and implications for plate boundary deformation, *J. Geophys. Res.*, *107*(B10), 2261, doi:10.1029/2001JB000282.
Benson, A., T. Little, R. Van Dissen, N. Hill, and D. Townsend (2001), Late Quaternary paleoseismic history and surface rupture characteristics of the eastern Awatere strike-slip fault, New Zealand, *Geol. Soc. Am. Bull.*, *113*(8), 1079–1091.
Bro, R., and S. D. Jong (1997), A fast non-negativity-constrained least squares algorithm, *J. Chemom.*, *11*, 392–401.
Carne, R., T. Little, and U. Rieser (2011), Using displaced river terraces to determine Late Quaternary slip rate for the central Wairarapa Fault at Waiohine River, New Zealand, *N. Z. J. Geol. Geophys.*, *54*(2), 217–236.
Costantini, M. (1998), A novel phase unwrapping method based on network programming, *IEEE Trans. Geosci. Remote Sens.*, *36*(3), 813–821.
Deng, J., and L. R. Sykes (1997), Stress evolution in southern California and triggering of moderate-, small-, and micro-size earthquakes, *J. Geophys. Res.*, *102*(B11), 24,411–24,435.
Du, W.-x., C. H. Thurber, M. Reyners, D. Eberhart-Phillips, and H. Zhang (2004), New constraints on seismicity in the Wellington region of New Zealand from relocated earthquake hypocentres, *Geophys. J. Int.*, *158*(3), 1088–1102.
Eberhart-Phillips, D., M. Reyners, S. Bannister, M. Chadwick, and S. Ellis (2010), Establishing a versatile 3-D seismic velocity model for New Zealand, *Seismol. Res. Lett.*, *81*(6), 992–1000.
Elliott, J., E. Nissen, P. England, J. A. Jackson, S. Lamb, Z. Li, M. Oehlers, and B. Parsons (2012), Slip in the 2010–2011 Canterbury earthquakes, New Zealand, *J. Geophys. Res.*, *117*(B3), B03401, doi:10.1029/2011JB008868.
Eshelby, J. D. (1957), The determination of the elastic field of an ellipsoidal inclusion, and related problems, *Proc. R. Soc. Ser. A*, *241*(1226), 376–396.
Farr, T., and M. Kobrick (2000), Shuttle radar topography mission produces a wealth of data, *EOS Trans. AGU*, *81*(48), 583–585, doi:10.1029/EO081i048p00583.
Goldstein, R. M., and C. L. Werner (1998), Radar interferogram filtering for geophysical applications, *Geophys. Res. Lett.*, *25*(21), 4035–4038.
Hamling, I. J., T. J. Wright, E. Calais, L. Bennati, and E. Lewi (2010), Stress transfer between thirteen successive dyke intrusions in Ethiopia, *Nat. Geosci.*, *3*, 713–717.
Harris, R. A., and R. W. Simpson (1996), In the shadow of 1857—The effect of the Great Ft. Tejon earthquake on subsequent earthquakes in southern California, *Geophys. Res. Lett.*, *23*(3), 229–232.
Holden, C., A. Kaiser, R. Van Dissen, and R. Jury (2013), Sources, ground motion, and structural response characteristics in Wellington of the 2013 Cook Strait earthquakes, *Bull. N. Z. Soc. Earthquake Eng.*, *46*(4), 188–195.
Holt, W. E., and A. Haines (1995), The kinematics of northern South Island, New Zealand, determined from geologic strain rates, *J. Geophys. Res.*, *100*(B9), 17,991–18,010.
Jónsson, S., H. Zebker, P. Segall, and F. Amelung (2002), Fault slip distribution of the 1999 M_w 7.1 Hector Mine, California earthquake, estimated from satellite radar and GPS measurements, *Bull. Seismol. Soc. Am.*, *92*, 1377–1389.
King, G. C. P., R. S. Stein, and J. Lin (1994), Static stress changes and the triggering of earthquakes, *Bull. Seismol. Soc. Am.*, *84*, 935–953.
Langbein, J. (2008), Noise in GPS displacement measurements from Southern California and Southern Nevada, *J. Geophys. Res.*, *113*, B05405, doi:10.1029/2007JB005247.
Langridge, R., and K. Berryman (2005), Morphology and slip rate of the Hurunui section of the Hope Fault, South Island, New Zealand, *N. Z. J. Geol. Geophys.*, *48*(1), 43–57.
Lensen, G. (1958), Note on fault correlations across Cook Strait, *N. Z. J. Geol. Geophys.*, *1*(2), 263–268.
Litchfield, N., et al. (2014), A model of active faulting in New Zealand, *N. Z. J. Geol. Geophys.*, *57*(1), 32–56, doi:10.1080/00288306.2013.854256.
Little, T., R. Van Dissen, E. Schermer, and R. Carne (2009), Late Holocene surface ruptures on the southern Wairarapa fault, New Zealand: Link between earthquakes and the uplifting of beach ridges on a rocky coast, *Lithosphere*, *1*(1), 4–28.
Mason, D. P., T. A. Little, and R. J. vanDissen (2006), Refinements to the paleoseismic chronology of the eastern Awatere Fault from trenches near Upcot Saddle, Marlborough, New Zealand, *N. Z. J. Geol. Geophys.*, *49*(3), 383–397.
Massonnet, D., and K. L. Feigl (1998), Radar interferometry and its application to changes in the Earth's surface, *Rev. Geophys.*, *36*, 441–500.
Massonnet, D., M. Rossi, C. Carmona, F. Adragna, G. Peltzer, K. Feigl, and T. Rabaute (1993), The displacement field of the Landers earthquake mapped by radar interferometry, *Nature*, *364*, 138–142.
Mountjoy, J. J., P. M. Barnes, and J. R. Pettinga (2009), Morphostructure and evolution of submarine canyons across an active margin: Cook Strait sector of the Hikurangi Margin, New Zealand, *Mar. Geol.*, *260*(1), 45–68.
Nicol, A., and J. Beavan (2003), Shortening of an overriding plate and its implications for slip on a subduction thrust, central Hikurangi Margin, New Zealand, *Tectonics*, *22*(6), 1070, doi:10.1029/2003TC001521.
Nodder, S. D., G. Lamarche, J.-N. Proust, and M. Stirling (2007), Characterizing earthquake recurrence parameters for offshore faults in the low-strain, compressional Kapiti-Manawatu Fault System, New Zealand, *J. Geophys. Res.*, *112*, B12102, doi:10.1029/2007JB005019.
Norris, R. J., and A. F. Cooper (2001), Late Quaternary slip rates and slip partitioning on the Alpine Fault, New Zealand, *J. Struct. Geol.*, *23*(2), 507–520.
Okada, Y. (1985), Surface deformation due to shear and tensile faults in a half-space, *Bull. Seismol. Soc. Am.*, *75*, 1135–1154.
Parsons, B., T. Wright, P. Rowe, J. Andrews, J. Jackson, R. Walker, M. Khatib, M. Talebian, E. Bergman, and E. R. Engdahl (2006), The 1994 Sefidabeh (eastern Iran) earthquakes revisited: New evidence from satellite radar interferometry and carbonate dating about the growth of an active fold above a blind thrust fault, *Geophys. J. Int.*, *164*, 202–217, doi:10.1111/j.1365-246X.2005.02655.x.
Pedersen, R., S. Jónsson, T. Árnadóttir, F. Sigmundsson, and K. L. Feigl (2003), Fault slip distribution of two June M_W6.5 earthquakes in South Iceland estimated from joint inversion of InSAR and GPS measurements, *Earth Planet. Sci. Lett.*, *213*, 487–502.

Pondard, N., and P. M. Barnes (2010), Structure and paleoearthquake records of active submarine faults, Cook Strait, New Zealand: Implications for fault interactions, stress loading, and seismic hazard, *J. Geophys. Res.*, *115*, B12320, doi:10.1029/2010JB007781.

Reasenberg, P. A., and R. W. Simpson (1992), Response to regional seismicity to the static stress change produced by the Loma Prieta earthquake, *Science*, *255*, 1687–1690.

Ristau, J. (2013), Update of regional moment tensor analysis for earthquakes in New Zealand and adjacent offshore regions, *Bull. Seismol. Soc. Am.*, *103*(4), 2520–2533.

Robinson, R. (2004), Potential earthquake triggering in a complex fault network: The northern South Island, New Zealand, *Geophys. J. Int.*, *159*(2), 734–748.

Segall, P. (2002), Integrating geologic and geodetic estimates of slip rate on the San Andreas fault system, *Int. Geol. Rev.*, *44*(1), 62–82.

Stevens, G. R. (1974), *Rugged Landscape: The Geology of Central New Zealand, Incl. Wellington, Wairarapa, Manawatu and the Marlbrough Sounds*, A. H. and A. W. Reed, Wellington, New Zealand.

Stirling, M., et al. (2012), National seismic hazard model for New Zealand: 2010 update, *Bull. Seismol. Soc. Am.*, *102*(4), 1514–1542.

Sutherland, R., K. Berryman, and R. Norris (2006), Quaternary slip rate and geomorphology of the Alpine fault: Implications for kinematics and seismic hazard in southwest New Zealand, *Geol. Soc. Am. Bull.*, *118*(3–4), 464–474.

Townsend, D., and T. Little (1998), Pliocene-Quaternary deformation and mechanisms of near-surface strain close to the eastern tip of the Clarence Fault, northeast Marlborough, New Zealand, *N. Z. J. Geol. Geophys.*, *41*(4), 401–417.

Van Dissen, R., and A. Nicol (2009), Mid-late Holocene paleoseismicity of the eastern Clarence Fault, Marlborough, New Zealand, *N. Z. J. Geol. Geophys.*, *52*(3), 195–208.

Van Dissen, R., and R. S. Yeats (1991), Hope fault, Jordan thrust, and uplift of the seaward Kaikoura Range, New Zealand, *Geology*, *19*(4), 393–396.

Van Dissen, R., et al. (2013), Landslides and liquefaction generated by the Cook Strait and Lake Grassmere earthquakes: A reconnaissance report, *Bull. N. Z. Soc. Earthquake Eng.*, *46*(4), 196–200.

Van Dissen, R. J., and K. R. Berryman (1996), Surface rupture earthquakes over the last 1000 years in the Wellington region, New Zealand, and implications for ground shaking hazard, *J. Geophys. Res.*, *101*(B3), 5999–6019.

Walcott, R. (1984), The kinematics of the plate boundary zone through New Zealand: A comparison of short- and long-term deformations, *Geophys. J. R. Astron. Soc.*, *79*(2), 613–633.

Wallace, L., B. Fry, S. C. Bannister, I. J. Hamling, Y. Ito, and K. Obara (2013), Large short- and long-term Hikurangi margin, New Zealand SSEs in 2013, and possible triggering of moderate to large seismicity during the SSEs, Abstract T44B-06 presented at 2013 AGU Fall Meeting Abstracts. [Available at http://adsabs.harvard.edu/abs/2013AGUFM.T44B..06W.]

Wallace, L. M., et al. (2009), Characterizing the seismogenic zone of a major plate boundary subduction thrust: Hikurangi Margin, New Zealand, *Geochem. Geophys. Geosyst.*, *10*, Q10006, doi:10.1029/2009GC002610.

Wallace, L. M., P. Barnes, J. Beavan, R. Van Dissen, N. Litchfield, J. Mountjoy, R. Langridge, G. Lamarche, and N. Pondard (2012), The kinematics of a transition from subduction to strike-slip: An example from the central New Zealand plate boundary, *J. Geophys. Res.*, *117*, B02405, doi:10.1029/2011JB008640.

Wallace, L. M., J. Beavan, R. McCaffrey, and D. Darby (2004), Subduction zone coupling and tectonic block rotations in the North Island, New Zealand, *J. Geophys. Res.*, *109*, B12406, doi:10.1029/2004JB003241.

Wallace, L. M., J. Beavan, S. Bannister, and C. Williams (2012), Simultaneous long-term and short-term slow slip events at the Hikurangi subduction margin, New Zealand: Implications for processes that control slow slip event occurrence, duration, and migration, *J. Geophys. Res.*, *117*, B11402, doi:10.1029/2012JB009489.

Wegmüller, U., and C. Werner (1997), Gamma SAR processor and interferometry software, in *Proceedings of the 3rd Symposium on Space at the Service of Our Environment, Florence, Italy*, (ESA SP-414), pp. 1687–1692, Estec, Noordwijk, Netherlands.

Williams, C. A., D. Eberhart-Phillips, S. Bannister, D. H. Barker, S. Henrys, M. Reyners, and R. Sutherland (2013), Revised interface geometry for the Hikurangi subduction zone, New Zealand, *Seismol. Res. Lett.*, *84*(6), 1066–1073.

Wright, T. J., B. E. Parsons, J. A. Jackson, M. Haynes, E. J. Fielding, and P. C. England (1999), Source parameters of the 1 October 1995 Dinar (Turkey) earthquake from SAR interferometry and seismic bodywave modelling, *Earth Planet. Sci. Lett.*, *172*, 23–37.

Zachariasen, J., K. Berryman, R. Langridge, C. Prentice, M. Rymer, M. Stirling, and P. Villamor (2006), Timing of late Holocene surface rupture of the Wairau fault, Marlborough, New Zealand, *N. Z. J. Geol. Geophys.*, *49*(1), 159–174.